Structure of B-DNA with Cations Tethered in the Major Groove[†,‡]

Tinoush Moulaei,[§] Tatsuya Maehigashi,[§] George T. Lountos,[§] Seiji Komeda,[§] Derrick Watkins,[§] Michael P. Stone,[∥] Luis A. Marky,[⊥] Jian-sen Li,[#] Barry Gold,[⊥,#] and Loren Dean Williams*[,§]

School of Chemistry and Biochemistry, Georgia Institute of Technology, Atlanta, Georgia 30332-0400, Department of Chemistry, Vanderbilt University, Nashville, Tennessee 37235, and Department of Pharmaceutical Sciences, University of Nebraska Medical Center, Omaha, Nebraska 68198, Eppley Institute for Research in Cancer, University of Nebraska Medical Center, Omaha, Nebraska 68198

Received January 21, 2005; Revised Manuscript Received March 29, 2005

ABSTRACT: Here, we describe the 1.6-Å X-ray structure of the DDD (Dickerson−Drew dodecamer), which has been covalently modified by the tethering of four cationic charges. This modified version of the DDD, called here the DDD^{4+}, is composed of $[d(CGCGAAXXCGCG)]_2$, where X is effectively a thymine residue linked at the 5 position to an *n*-propyl-amine. The structure was determined from crystals soaked with thallium(I), which has been broadly used as a mimic of K^+ in X-ray diffraction experiments aimed at determining positions of cations adjacent to nucleic acids. Three of the tethered cations are directed radially out from the DNA. The radially directed tethered cations do not appear to induce structural changes or to displace counterions. One of the tethered cations is directed in the 3′ direction, toward a phosphate group near one end of the duplex. This tethered cation appears to interact electrostatically with the DNA. This interaction is accompanied by changes in helical parameters rise, roll, and twist and by a displacement of the backbone relative to a control oligonucleotide. In addition, these interactions appear to be associated with displacement of counterions from the major groove of the DNA.

DNA conformation is influenced by a variety of factors. In a ground-state DNA structure, interactions of water molecules with the hydrophobic surfaces of DNA bases are minimized, stacking and hydrogen-bonding interactions are maximized, and intramolecular phosphate−phosphate repulsions are minimized. DNA sequence is an important modulator of DNA structure. A-tracts are associated with narrow minor grooves (*1*−*3*), axial bends (*4*−*6*), and high propeller twists (*7*). G-tracts show a strong divalent cation dependence of bending (*8*, *9*) and a propensity to convert to A-form (*10*−*12*). The sequence dependence of DNA conformation can be ascribed to base-specific hydrophobicity, shape, charge distribution, and functional group disposition. The relative importance and mechanisms by which various sequence-specific factors influence DNA conformation is not currently resolved.

Here, we examine the X-ray structure of the Dickerson−Drew dodecamer (DDD)[1] that has been covalently modified by the tethering of four cationic charges. This modified version of the DDD, called here the DDD^{4+}, is composed of $[d(CGCGAAXXCGCG)]_2$, where X is effectively a thymine residue linked at the 5 position to an *n*-propyl-amine (Z3dU, Figure 1). The four *n*-propyl-amino groups of DDD^{4+} are protonated under the conditions of our experiments. The 4^+ of DDD^{4+} represents the charge of the four modifications. The net charge of the DDD^{4+}, including contributions from phosphate groups, is 18^-.

The goal of the work here is to determine the effects of tethered cations on DNA conformation and on distribution of nontethered cations such as K^+, Mg^{2+}, and spermine. To determine nontethered cation positions, the structure of DDD^{4+} was determined in the presence of Tl^+ ions. Thallium(I), with a strong anomalous signal, has been broadly used as a mimic of K^+ in X-ray diffraction experiments aimed at determining positions of cations adjacent to nucleic acids (*13*−*15*) and proteins (*16*−*25*). In previous work from our laboratory, 13 Tl^+ sites were identified in the solvent region of the unmodified form of the DDD (native DDD) (*13*). We refer to this structure as DDD-Tl^+. Here, we present evidence that tethering of cations in the major groove influences DNA deformation and the distribution of the counterion Tl^+.

The motivation for this work stems from work of Mirzabeckov, Rich, and Manning (*26*, *27*), who considered the proposition that charge neutralization of phosphate groups might drive DNA bending. They were concerned with asymmetric charge neutralization by cationic protein side chains, leading to "phosphate collapse". That model was

[†] This work was supported by the National Science Foundation (Grant MCD-9976498).

[‡] Coordinates have been submitted to NDB (entry BD0075).

* To whom correspondence should be addressed. E-mail: loren.williams@chemistry.gatech.edu. Telphone: (404) 894-9752. Fax: (404) 894-7452.

[§] Department of Chemistry and Biochemistry, Georgia Institute of Technology.

[∥] Department of Chemistry, Vanderbilt University.

[⊥] Department of Pharmaceutical Sciences, University of Nebraska Medical Center.

[#] Eppley Institute for Research in Cancer, University of Nebraska Medical Center.

[1] Abbreviations: DDD, Dickerson−Drew dodecamer, $[d(CGCGAATTCGCG)]_2$; DDD^{4+}, DDD containing four Z3dU residues and soaked with Tl^+, $[d(CGCGAAXXCGCG)]_2$, (X = Z3dU); DDD-Tl^+, DDD grown in the presence of Tl^+; Z3dU, 5-(3-aminopropyl)-2′-deoxyuridine.

10.1021/bi050128z CCC: $30.25
Published on Web 04/30/2005

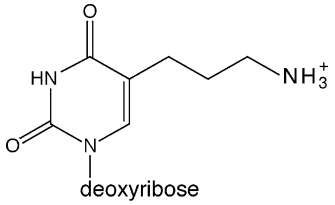

FIGURE 1: Chemical structure of Z3dU. The cationic amino nitrogen is referred to here as N^+.

extended by Rouzina and Bloomfield (*28*), who proposed that mobile cations such as Mg^{2+} can contribute electrostatically to DNA bending. In the Rouzina and Bloomfield model, a divalent cation can repel and displace other counterions, leading to strong attraction with unscreened phosphate groups. The result is DNA bending by electrostatic collapse around a divalent cation. Our experimental system, with short oligonuclotides, has limitations for analysis of DNA bending. However, it does provide a detailed view of microheterogenity in DNA conformation and complements NMR studies (*29*) using the same modified oligonucleotide studied here.

MATERIALS AND METHODS

Crystallization. Reverse-phase HPLC purified d(CGCGAAXXCGCG) was synthesized and purified as described (*30*). The oligomer was annealed by slow cooling from 80 °C. Crystals were grown over 2−3 days using the sitting drop vapor diffusion method. The crystallization solution contained 0.6 mM DNA (duplex), 20 mM spermine cacodylate (pH 6.5), 4.0% (v/v) 2-methyl-2,4-pentanediol (MPD), 4.0 mM spermine acetate (pH 6.5), and 20% (v/v) ANAPOE-$C_{12}E_{10}$ (Hampton Research). The DNA concentration was determined by UV absorbance, assuming that the modifications do not affect the extinction coefficient. The crystallization solutions were equilibrated against a reservoir of 35% (v/v) MPD at 22 °C. The spermine cacodylate solution was prepared by titrating a solution of cacodylic acid (Sigma) with a solution of spermine base (Sigma). The concentration of spermine in the initial crystallization solution, including contributions from the spermine-cacodylate solution, was 8.0 mM. Efforts to grow crystals of dCGCGAAXXCGCG in the presence of Tl^+ were not successful. A wide range of pH, Mg^{2+}, spermine, and Tl^+ concentrations were assayed. It was concluded that dCGCGAAXXCGCG shows a propensity to crystallize only under low cationic strength. The conditions reported here are at the minimum limit of cation concentration that produces diffraction-quality crystals. Because it was not possible to grow high-quality crystals of dCGCGAAXXCGCG from solutions containing sufficient Tl^+, crystals were soaked with Tl^+. The initial soaking solution contained 40 mM thallium(I) acetate, 20 mM spermine·cacodylate (pH 6.5), 4.0% (v/v) MPD, 4 mM spermine acetate (pH 6.5), and 20% (v/v) ANAPOE-$C_{10}E_{12}$. Equivalent volumes of crystallization and the initial soaking solutions were equilibrated against a reservoir of 35% (v/v) MPD and combined to give the final soaking solution. A crystal of dimensions $0.1 \times 0.1 \times 0.1$ mm^3 was transferred to the final soaking solution. After 6 h, the crystal was looped and frozen in liquid nitrogen.

Data Collection and Processing. A total of 360° of data, with an oscillation angle of 1.0°, was collected at beamline 22-ID in the SER-CAT facilities at APS using a MAR-165 CCD detector at a wavelength of 1.009 30 Å. The crystal was maintained at −160 °C. Data were scaled and integrated using HKL2000 version 1.97.7 (*31*). Initial inspection of the images suggested twinning. The quality of the data was significantly improved by excluding a subset of bad frames, indicated by HKL2000 statistics. An initial round of integration and scaling was performed using all frames. A total of 146 309 reflections were indexed, integrated, and reduced to 8901 unique reflections with merged Bijoet pairs and 15 840 unique reflections with unmerged Bijoet pairs. Unit cell dimensions are $a = 24.99$, $b = 41.06$, and $c = 66.34$ Å, in space group $P2_12_12_1$. The data used in the refinement included 6586 unique reflections from 75 to 1.51 Å. Table 1 contains data collection and refinement statistics.

Table 1: Crystallographic and Refinement Statistics

unit cell	
a (Å)	24.99
b (Å)	41.06
c (Å)	66.34
space group	$P2_12_12_1$
temperature of data collection (°C)	−160.0
number of reflections	146 309
number of unique reflections	8901
completeness (%)/highest shell (%)	77.3/49.1
max resolution of observed reflections (Å)	1.49
max resolution of highest shell used (Å)	1.60
resolution range (Å)	35−1.60
number of reflections used in refinement	7355
number of reflections used in the test set	778
rmsd of bonds from ideal (Å)	0.0098
rmsd of angles from ideal (Å)	1.3809
DNA (asymmetric unit)	$[d(CGCGAAXXCGCG)]_2$
number of DNA atoms	498
number of water molecules	114
number of Mg^{2+} ions	0
number of spermine atoms	15 (2 partial molecules)
R free (%)	24.42
R factor (%) excluding test set data	19.80
unit cell volume occupied (%)	61.25

Refinement. Molecular replacement was used for phase determination. The coordinates for an unmodified starting DNA model [entry BDL084 (*32*)] were obtained from NDB (*33*). The program CNS version 1.1 (*34*) was used, along with the parameters of Berman and co-workers (*35*−*37*) for refinement. Parameter files were modified to remove dihedral restraints, except for the addition of dihedral restraints to keep the planarity of purine and pyrimidine ring systems. Parameters for Z3dU, estimated by combining elements of thymine and lysine, were incorporated into the parameter files. Initial electron-density maps and refinement statistics from starting model BDL084 indicated an incorrect solution. The structure was solved by a rotational/translational search and rigid-body refinement in CNS. At this stage, the position of the Z3dU modifications could be identified in the difference electron-density maps. The four thymine residues in structure BDL084 were converted to Z3dU. The resulting model was annealed and refined. Water molecules were added iteratively followed by annealing, refinement, and phase calculation using peaks in the sum $(2|F_o| - |F_c|)$ and difference $(|F_o| - |F_c|)$ maps. Anomalous $(|F^+| - |F^-|)$ maps showed the positions of Tl^+ ions. The initial phases for the anomalous map were obtained from the positions of DNA phosphorus atoms. Six possible Tl^+ sites were identified in

this map. Water molecules previously located at these sites were converted to partially occupied Tl^+ atoms. Successive refinements and map calculations were performed. Estimates of occupancies were obtained by monitoring negative and positive difference electron density. Additional anomalous maps were made using the position of the phosphorus atoms and the six partially occupied Tl^+ atoms to calculate phases. Three additional Tl^+ sites were thus identified. These sites where added to the model in the same manner as the first six; however, only two of these sites resulted in acceptable geometry and statistics. Helical parameters were calculated with Curves 5.3 (*38*).

RESULTS

DNA Conformation. The final model of DDD^{4+}, including the amino-propyl groups, is well-determined by the data (Figure 2). The occupancies of the two terminal O5′ atoms of the DNA were set to zero because they appear to be disordered; there is no electron density observed around them.

Each of the four amino-propyl modifications is readily identifiable in sum and difference maps (Figure 3). Three amino-propyl groups (on residues 7, 8, and 19) extend radially out from the DNA and into intermolecular cavities in the crystal. These cationic amino groups do not appear to engage in significant intramolecular interactions with the DNA backbone or bases.

The relative strength of various electrostatic forces between N^+ (N^+ refers to the cationic amino nitrogen of the amino-propyl of Z3dU) and phosphate oxygens (OP) of the DNA are indicated symbolically in Figure 4. Each circle in this figure represents a single N^+-OP distance. All distances less than 10 Å are indicated. The sizes of the circles are proportional to $1/r^2$, where r is the N^+ to OP distance. The blue and red circles indicate intraduplex distances. These interactions would be observed in an isolated duplex in solution, assuming that the conformation in the crystal and solution is conserved. The interactions of the N^+ of residue 20 ($20N^+$) are indicated by red circles in Figure 4. The amino-propyl modification of residue 20 extends in the 3′ direction. The $20N^+$ appears to be involved in significant electrostatic interactions with the DNA. These circles (red) are focused primarily at one end of the duplex. The phosphates on this end of the duplex are engaged in significant electrostatic interactions with the $20N^+$. The largest circle is adjacent to base pair 2−23 and indicates a distance of 6.4 Å. This interaction involves the O1P atom of G(2). The blue circles indicate intraduplex contacts of $7N^+$, $8N^+$, and $19N^+$ with OP atoms. These distances are relatively long and are evenly distributed over the duplex. A third set of circles (green) in Figure 4 represents interduplex interactions. These are "lattice interactions" between adjacent duplexes in the crystal. These interactions are focused at the end of the duplex opposing the $20N^+$ interactions. The largest green circle represents an interaction of 5.0 Å with the O2P atom of C(15). Because these lattice interactions are focused primarily at the end of the duplex with conserved conformation, it can be argued that they are not inducing the observed deformation.

The intraduplex electrostatic interaction of $20N^+$ with the DNA appears to distort the backbone and major groove

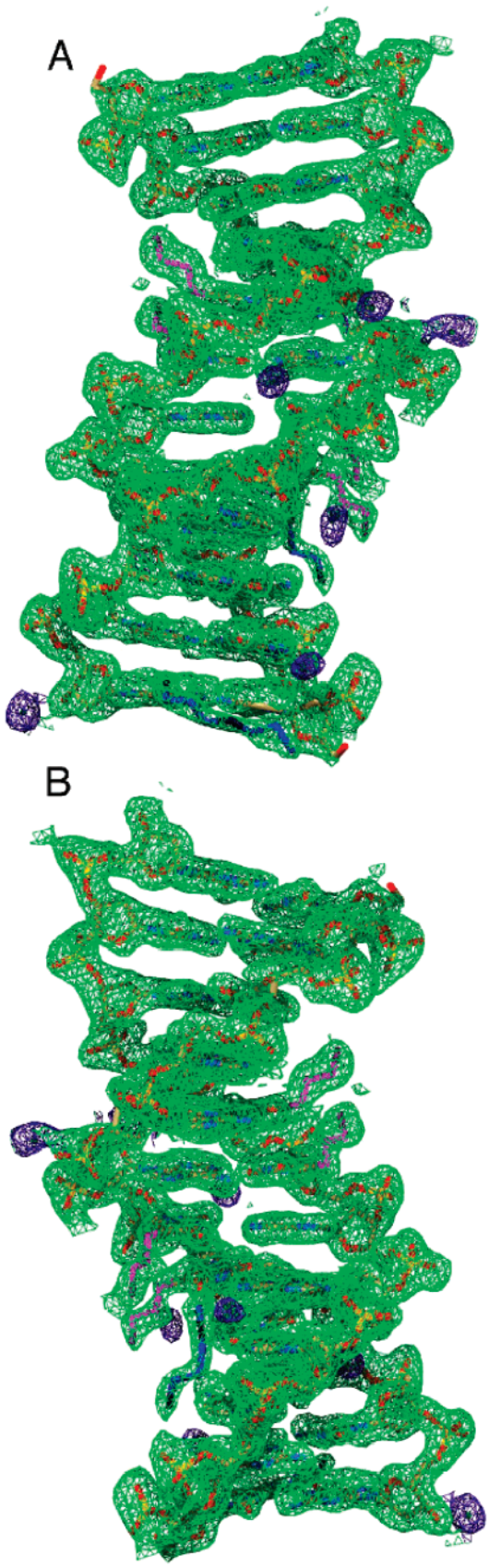

FIGURE 2: Sum electron density contoured at 1.0σ around the DDD^{4+}. The sum electron density is drawn as a green net everywhere except around the Tl^+ ions, where it is a blue net. (A) Minor groove. (B) Major groove (rotated by 180°). The amino-propyl modifications are in magenta, with the N^+ atoms in dark magenta. Two spermine molecules are colored in blue, with the nitrogen atoms in dark blue.

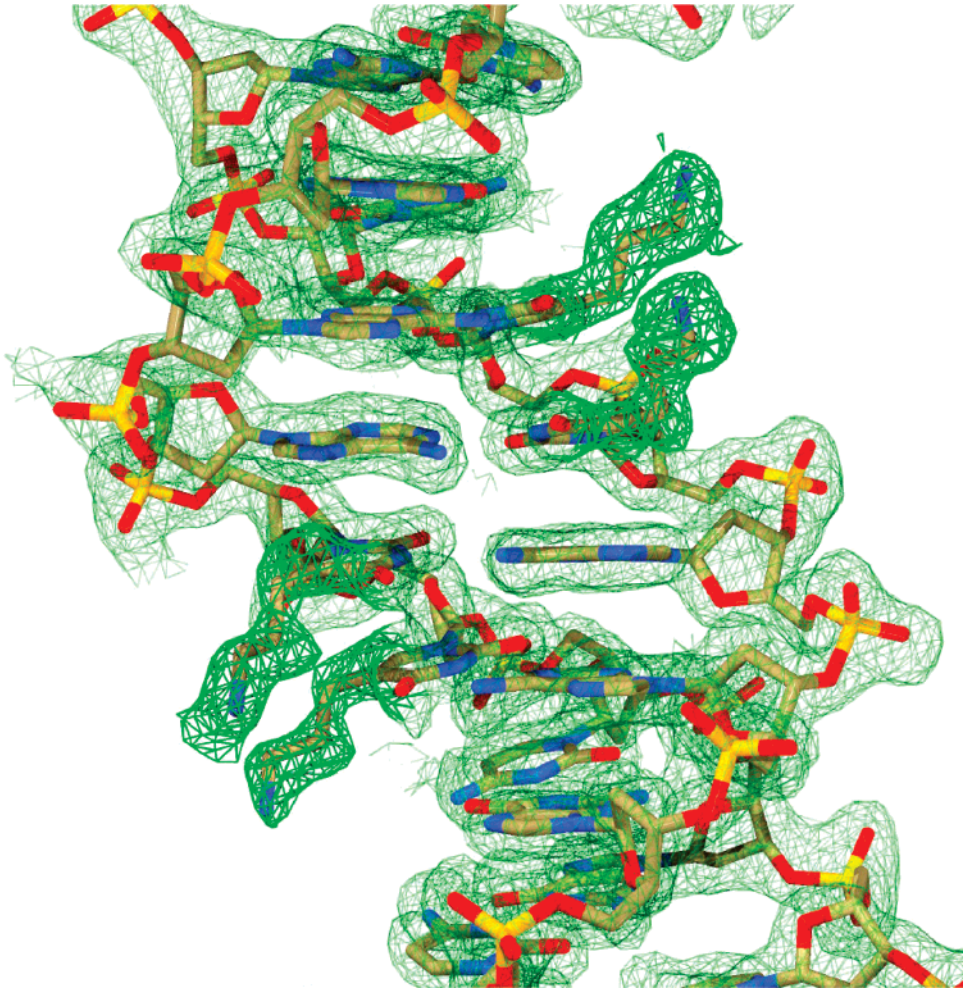

FIGURE 3: Close-up view of the sum electron density contoured at 1.0σ around the amino-propyl modifications of the four Z3dU residues. The density is drawn as a dark green net around the modifications and as a transparent green net elsewhere.

geometry. These distortions are inferred by comparing DDD^{4+} with native DDD structures. Here, we compare DDD^{4+} with a series of DDD structures determined from crystals obtained in the presence of various cations, in our laboratory. The members of this ensemble were determined independently and give an indication of the minimum accuracy of the helical parameters. Some important helical parameters are shown in Figure 4. It can be seen that the rise, roll, and helical twist of DDD^{4+} are different from those of the native DDD ensemble. One-half of the DDD^{4+}, from base pairs 6−19 to 12−13, is representative of the ensemble and does not deviate significantly from it. However, the other half of DDD^{4+}, from base pairs 1−24 to 5−20, does deviate from the DDD ensemble. The deviations are localized primarily to base pairs 2−23 and 3−22. The helical rise of DDD^{4+} at the step from base pair 2−23 to base pair 3−22 is 3.4 Å, which is significantly less than the 3.7 Å rise observed for the ensemble. At the same step, the roll of DDD^{4+} (0°) is over 10° greater than the ensemble average (less than −11°). Similarly, at this step, the helical twist of the DDD^{4+} (34°) is much less than the ensemble average (42°). The important point of this analysis is that the deviations of DDD^{4+} from the DDD ensemble are localized to the region where the intermolecular interaction of tethered cation with the DNA phosphate groups is most significant. The widths of the major and minor grooves and the depth of the major groove of DDD^{4+} are similar to the rest of the DDD ensemble. The depth of the minor groove of DDD^{4+} deviates from the DDD ensemble in the bent half of of the duplex.

A superimposition of DDD^{4+} with DDD-Tl^{+} is shown in Figure 5. The differences between the two DNA duplexes are limited primarily to the region of interaction of the amino group of Z3dU(20) with DNA phosphate groups. The greatest atomic displacements of DDD^{4+} compared to DDD-Tl^{+} is in residues 1 and 2 in one strand and residues 21−24 in the complementary strand. The deviation between the two structures is greatest in backbone atoms. An asymmetric displacement of the two strands has resulted in an asymmetric collapse of the major groove in this terminus.

In addition, difference density near the O1P and O2P of G(2) suggests that this phosphate group is positionally disordered. The phosphate group appears to occupy several positions along a trajectory in and out of the major groove. This disorder is indicated by difference peaks in the electron-density maps. These maps are shown in Figure 6 along with details of the interaction between the N^{+} of Z3dU(20) and the OP atoms. Table 2 lists the relevant distance and angle information. A water molecule [$H_2O(96)$] bridges $20N^{+}$ and O1P of G(2) and O2P of Z3dU(7) of a symmetry-related duplex. At its closest approach, the distance between the O1P of G(2) and the N^{+} is estimated to be 4.9 Å. This distance was estimated from the position of the N^{+} atom and the center of the difference peak near the O1P of G(2).

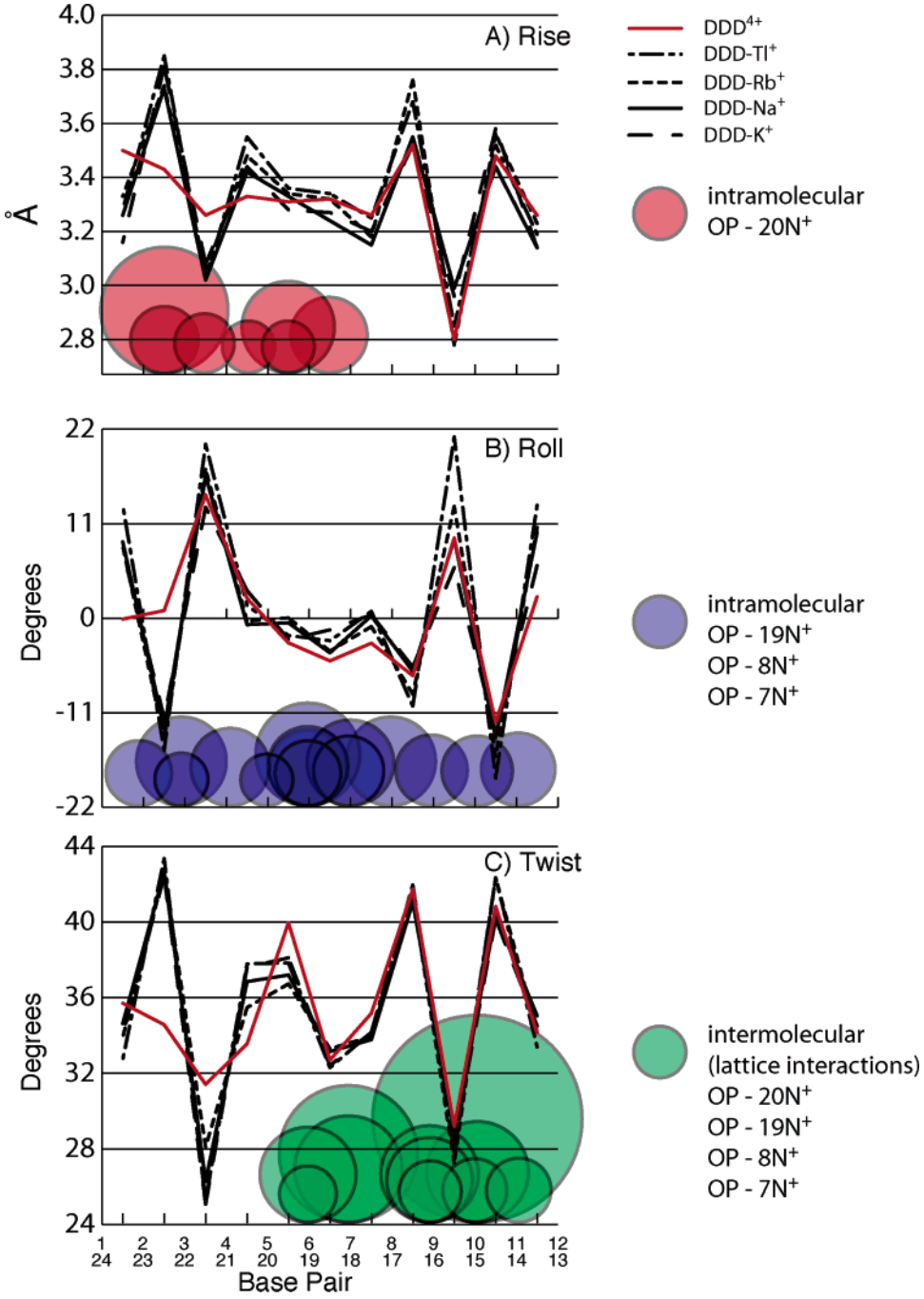

FIGURE 4: Interbase pair parameters and N^+−OP proximities. (A) Helical rise, (B) base-pair roll, and (C) helical twist for DDD^{4+} and several structures of DDD. The solid red lines indicate the values for DDD^{4+}. The circles indicate the proximity of N^+ to OP within the same duplex (red and blue) or O1P/O2P of a symmetry-related molecule (green). The red circles indicate the proximity of $20N^+$. The blue circles indicate the proximity of $6N^+$, $7N^+$, and $19N^+$. The radii of the circles are scaled by $1/r^2$, where r is the distance between N^+ and OP. The largest red circle corresponds to the shortest contact, which is a contact between $20N^+$ and O1P of residue 2. The DDD structures were obtained from crystals grown in the presence of a variety of monovalent cations and low concentrations of Mg^{2+}.

$H_2O(96)$ is 1.1 Å below the plane of N^+, O1P, and O2P. Therefore, it only partially screens N^+ from O1P of residue 2. Directly below this water molecule (2.4 Å) is another water molecule [$H_2O(60)$]. Although not modeled in this way, it is possible that $H_2O(60)$ and $H_2O(96)$ are partially occupied and are effectively the same water molecule at two different positions. It seems likely that, when the phosphate of G(2) swings into the major groove, the bridging water molecule moves deeper into the groove.

Counterions. In the final model, the solvent region of DDD^{4+} contains 114 water molecules, eight partially occupied Tl^+ ions, and two partially ordered spermine molecules. The anomalous electron-density map shows peaks from the eight Tl^+ sites and from the DNA phosphorus atoms (Figure 7). The occupancies of the Tl^+ ions range from 0.15 to 0.22 with a summed occupancy of 1.35.

We have allocated the eight observed Tl^+ sites of DDD^{4+} to three classes: *conserved*, *semiconserved*, and *variable* (Tables 3 and 4). This classification scheme is based on similarities and differences in the Tl^+ position of DDD^{4+} versus DDD-Tl^+. The Tl^+ sites of DDD-Tl^+ were determined previously from crystals grown in the presence of thallium-

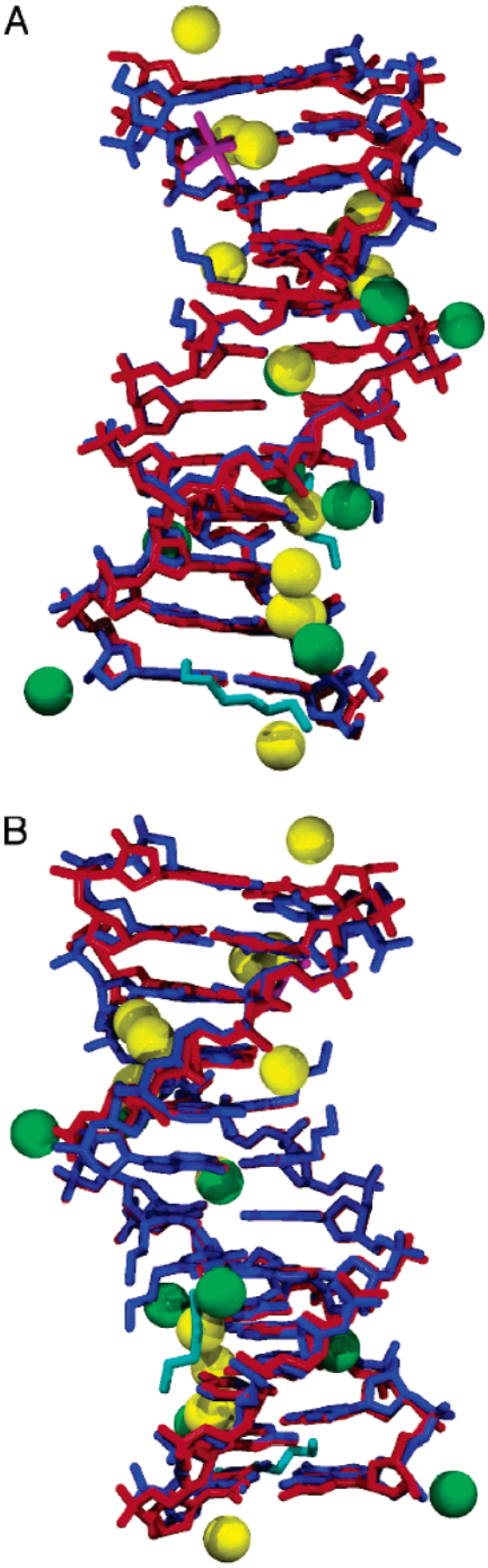

FIGURE 5: Superimposed structures of the DDD^{4+} (blue, with green Tl^+ ions) and DDD (red, with yellow Tl^+ ions). The spermine molecules are in cyan. The $Mg^{2+}(H_2O)_6$ complex is in magenta. (A) Minor groove. (B) Major groove (rotated by 180°).

(I) acetate (*13*). *Conserved* DDD^{4+} Tl^+ ions are less than 1 Å from a Tl^+ ion in DDD-Tl^+. *Semiconserved* DDD^{4+} Tl^+ ions are between 1.0 and 4.0 Å from one or more Tl^+ ions in DDD-Tl^+. Finally, *variable* DDD^{4+} Tl^+ ions are greater than 4.0 Å from any Tl^+ ion in DDD-Tl^+. Proximities were determined by superimposing DDD^{4+} onto DDD-Tl^+, as shown in Figure 5, then applying symmetry, and then taking differences in positions.

Only one Tl^+ site of DDD^{4+} falls in the *conserved* class. A Tl^+ ion is located in the minor groove of both DDD^{4+} and DDD-Tl^+, at the ApT step. A Tl^+ ion with occupancy of 0.15 in the DDD^{4+} makes contacts with four DNA oxygen atoms (two O2 atoms and two O4′ atoms) and two solvent sites. This hexacoordinate site is called the P3 site (*39*, *40*) and is occupied by monovalent cations in a series of crystallographic studies of DDD, by a variety of cations (K^+, Rb^+, Cs^+, and Tl^+) (*13*, *39*−*42*).

Of the remaining seven Tl^+ sites of DDD^{4+}, two are *semiconserved* and five are *variable*. In general, the sites in the minor groove are either *conserved* or *semiconserved*, while the sites in the major groove are *variable*. The variability of these sites in the major groove is expected, because that is where the tethered cations are located. In fact the major groove of DDD^{4+} contains fewer cations than the major groove of DDD-Tl^+. There are three Tl^+ ions in the major groove of the modified structure (28, 33, and 34), of which Tl(28) is well above the opening of the groove and should not be considered "inside" the groove. In comparison, there are seven Tl^+ ions in the major groove of DDD-Tl^+ (2101, 2102, 2103, 2107, 2108, 2110, and 2114). Tl(2107) and Tl(2108) are in a region partially occupied by an Mg^{2+} coordinated with six water molecules. DDD^{4+} lacks an Mg^{2+} ion at this position. This is not necessarily an indication of altered electrostatic environment because DDD^{4+} was crystallized in the absence of Mg^{2+}. Whether this specific site can be occupied by an Mg^{2+} in DDD^{4+} structure must be determined through further experiments. However, the results obtained thus far do indicate that cations appear to have been expelled from the major groove, especially from the vicinity of $20N^+$. Some of the differences in Tl^+ distribution between DDD^{4+} and DDD-Tl^+ may arise from the methods used to introduce Tl^+ ions into the crystals. The DDD^{4+} structure was soaked in Tl^+, while the DDD-Tl^+ crystal was grown from a solution containing Tl^+.

The Tl^+ at the P3 site in the minor groove is conserved in both structures (Figure 5). It appears to have similar occupancies, 0.15 in the modified and 0.10 in the unmodified structures. Table 4 contains the contact information for all of the Tl^+ ions. There are three Tl^+ ions in the major groove of DDD-Tl^+, near the bending region (2103, 2107, and 2108). Tl(2107) and Tl(2108) are at the same site that is partially occupied by an Mg^{2+} ion. In the DDD^{4+} structure, there is only one Tl^+ ion (32) nearby, which is well above the major groove at a distance of 4.96 Å from $20N^+$. At the other terminus, there are four Tl^+ ions in the DDD-Tl^+ structure (2101, 2102, 2110, and 2113) and two in the DDD^{4+} (33 and 34). Tl(2102) and Tl(2113) sites overlap and are mostly likely the same cation in two different positions. Tl(33) and Tl(34) do not contact the floor of the major groove. Tl(33) is 6.24 Å from $7N^+$, and Tl(34) is 5.54 Å from $8N^+$. Another effect of this cation redistribution can be seen in the occupancies (Table 4). The total monovalent cation oc-

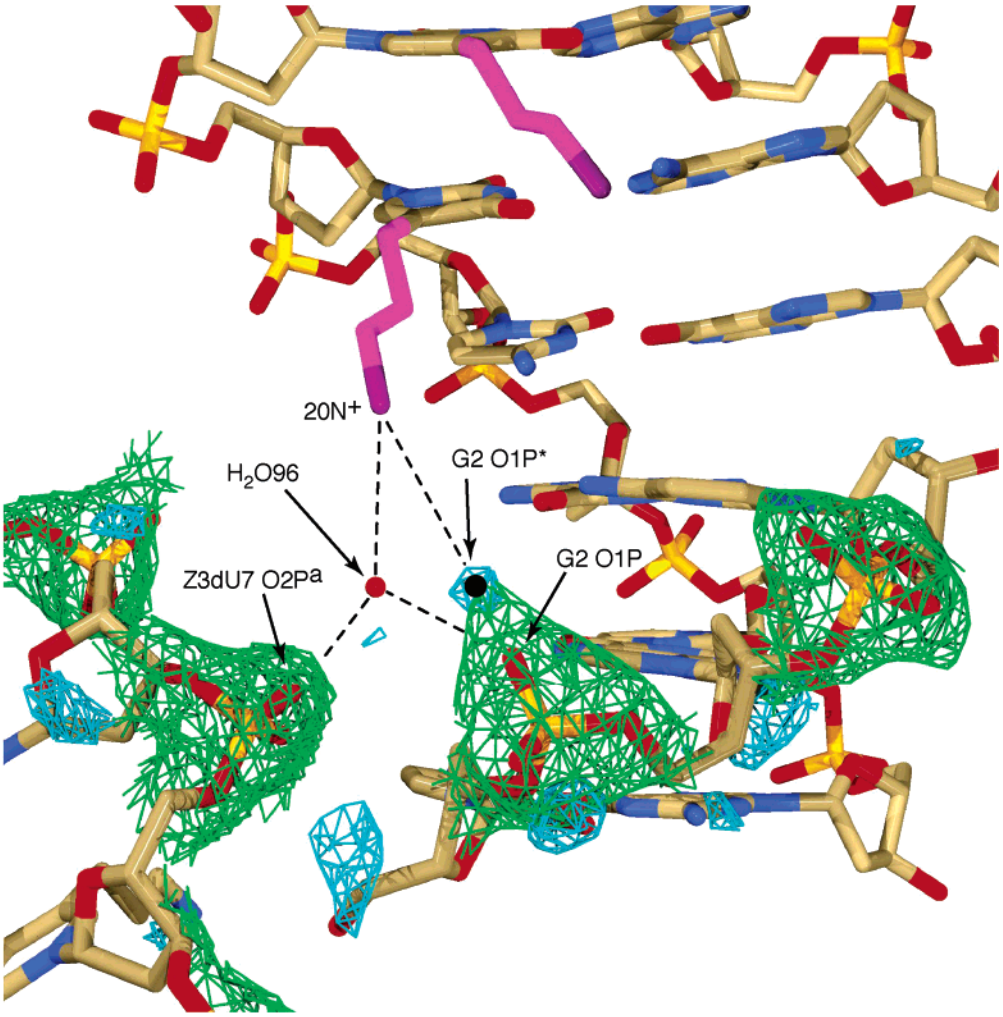

FIGURE 6: Close-up view of the contact between $20N^+$ and the backbone of the same molecule and a symmetry-related molecule. Sum electron density (1.0σ) and difference electron density (2.5σ) are drawn around the phosphate groups. The sum density is in a green net, and the difference density is in a cyan net. Refer to Table 3 for distances and angles.

Table 2: Distances and Angles for Z3dU 20

distances (Å)		angles (deg)	
N^+-H_2O	3.59	N^+-H_2O-O1P	112
$O1P-H_2O$	4.13	N^+-H_2O-O2P	135
$O2P-H_2O$	3.05	$O1P-H_2O-O2P$	85
N^+-O1P	6.40		
N^+-O2P^a	6.14		
N^+-O1P^{*b}	4.91		

[a] This is from a symmetry-related duplex. [b] O1P* is the alternative position for O1P, where it is at its closest approach to $20N^+$. This position is at the center of the difference peak near O1P.

cupancy in the minor groove is reasonably similar between the two structures (DDD^{4+}, 0.74; DDD-Tl^+, 0.60). However, the total monovalent cation occupancy is reduced in the major groove (DDD^{4+}, 0.30; DDD-Tl^+, 1.34). Interestingly, the total charge in the distorted region of the major groove is constant between the two structures (+2.0). This is considering the partially occupied Mg^{2+} ion and the two amino-propyl modifications. However, in DDD-Tl^+, the charged atoms are distributed on the bottom of the major groove and are in contact with the floor of the major groove, while in DDD^{4+}, the charged species are well above the floor and distributed along the upper region of the major groove. Some of these differences in Tl^+ localization may arise from differences in crystallization procedures. DDD-Tl^+ crystals were grown in the presense of Tl^+, while DDD^{4+} crystals were soaked with Tl^+.

The final model of DDD^{4+} contains two partial spermine molecules labeled spermine(26) and spermine(27). The portions of these molecules that are disordered are not visible in the electron-density maps and were not included in the model. The sum electron density surrounding the spermine molecules is shown in Figure 8. Models in which the spermine molecules are replaced with water molecules show worse statistics and inferior maps. Refinement of a model omitting the spermine molecules resulted in strong (greater than 3.5σ) difference electron density at their location. Both spermine molecules are located in the G-tract major groove on the end of the duplex where the conformation of DDD^{4+} is similar to that of native DDD. Spermine(25) lies at the mouth of the major groove, making contacts with an adjacent DNA molecule. Spermine(26) extends outward from the major groove and is aligned with the amino-propyl modifications of Z3dU(7) and Z3dU(8). In the cavity occupied by this spermine molecule and the two amino-propyl groups, there are ordered water molecules in the region proximal to the modifications, but none can be identified in the distal region of the cavity. It is likely that disordered solvent molecules and perhaps the remainder of spermine(26) occupy the rest of this cavity.

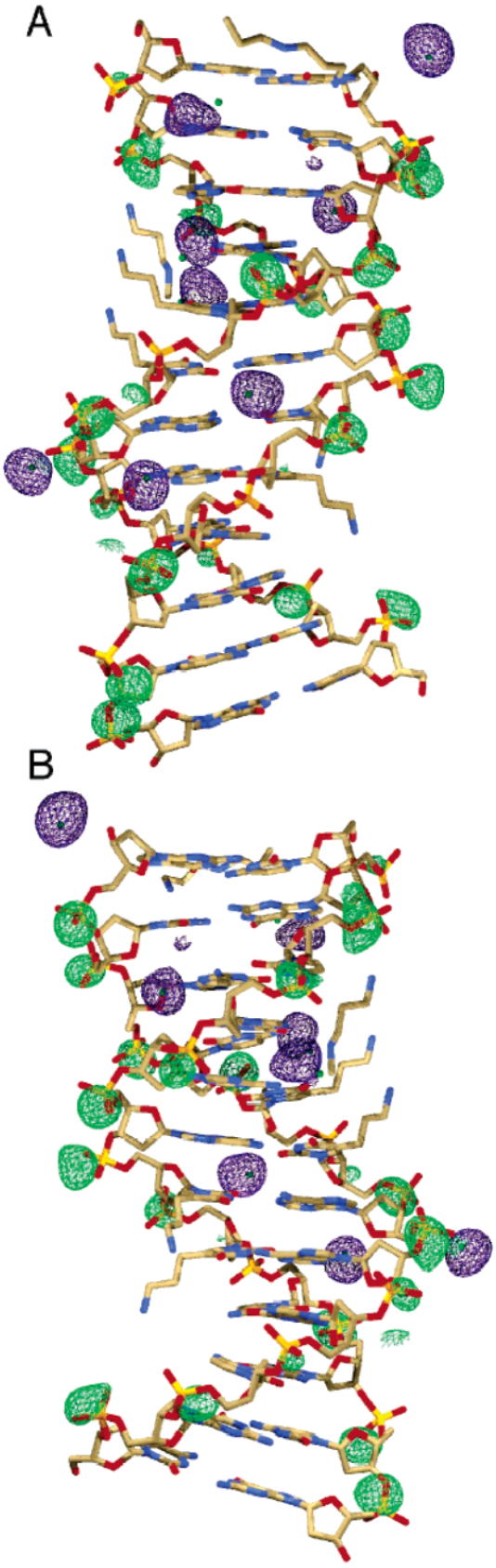

FIGURE 7: Anomalous density contoured at 2.5σ around DDD^{4+}. The density around all atoms is drawn as a green net, except for Tl^+ ions, where it is drawn as a blue net. The map was calculated using only the positions and occupancies of the 8 Tl^+ ions. The observed peaks around the phosphorus atoms sever as a positive control. (A) Minor groove. (B) Major groove (rotated by 180°).

Table 3: Classification and Location of DDD^{4+} Tl^+ Ions

class[a]	Tl^+ in DDD^{4+}	Tl^+ in DDD	distance (Å)	location of Tl^+ in DDD^{4+}
C	30	2106	0.22	minor groove, ApT step
S	31	2104	3.04	minor groove
S	27	2105	3.50	minor groove
V	34	2101	4.80	major groove
V	33	2110	4.91	major groove
V	28	2113	5.02	above major groove
V	28	2110	5.57	
V	28	2102	5.97	
V	29		>6	minor groove
V	32		>6	edge of major groove

[a] C, conserved; S, semiconserved; V, variable.

There are two components in the crystallization solution with the topology of an unbranched chain, spermine, and the detergent ANAPOE-$C_{12}E_{10}$ [polyoxyethylene(10)dodecyl ether]. As partial molecules, they may be difficult to distinguish. The electron density associated with the spermine molecules might also be modeled as partial detergent molecules. However, the detergent molecules are 42 atoms long and more hydrophobic than spermine. Spermine appears to be the more logical choice for the confined, hydrophilic environment of the intermolecular cavities of the crystal.

DISCUSSION

Double helical DNA is a semirigid polymer with a persistence length of 140−150 base pair (*43*, *44*). Under certain conditions, DNA can be induced to bend spontaneously. DNA bends away from TATA-element binding protein (TBP) by almost 90° (*45*, *46*). DNA bends toward catabolite activator protein (CAP) by around 90° (*47*). In the nucleosome core particle, DNA wraps around a complex of histone proteins by nearly two full turns (*48*−*50*).

Many of these DNA distortions can be explained by the electrostatic collapse model of Mirzabeckov, Rich, and Manning. In one test of that model, "phantom proteins" were created by Maher et al. (*51*−*55*). DNA was covalently tethered to cations, i.e., phantom proteins. Maher et al. also partially neutralized DNA by modification of phosphates. From the effects of the phantom proteins on the electrophoretic mobility of DNA, it was concluded that axial bending can be caused by interactions of charged species with DNA. Appropriate cation adduction or phosphate neutralization induces spontaneous bending of DNA, suggesting the importance of asymmetric charge neutralization.

The effects of tethered cations on the three-dimensional structure of DNA at high resolution have been studied by Li et. al., who obtained NMR results using the singly modified $[d(CGCGAATXCGCG)]_2$ (DDD^{2+}) molecule. The results are consistent with DNA deformation, including axial bending (*29*). The NMR data suggest an ordered environment for the Z3dU moiety within the major groove. The aminopropyl group appears to extend in the 3′ direction, accompanied by a perturbation of the phosphodiester backbone of the DDD^{2+} molecule. This perturbation is indicated by a chemical-shift perturbation of the ^{31}P resonance of the relevant phosphodiester linkage. The DNA deformations were attributed to an electrostatic interaction between phosphates and the tethered cationic charge.

In the DDD^{4+} structure described here, four positively charged amino groups are tethered to the major groove of

Table 4: Positions and Occupancies of DDD and DDD^{4+} Tl^+ Ions

molecule	DDD^{4+}			DDD		
region	minor	major	other	minor	major	other
Tl^+ ion[a]	27 (0.22) 29 (0.20) 30 (0.16)[c] 31 (0.16)	33 (0.15) 34 (0.15)	32 (0.15) 28 (0.15)	2104 (0.20)[b] 2105 (0.18)[b] 2106 (0.10)[c] 2109 (0.12)[b]	2101 (0.34) 2102 (0.29) 2103 (0.20) 2107 (0.10)[b] 2108 (0.10)[b] 2110 (0.15) 2113 (0.16)	2111 (0.18) 2112 (0.15)
total[d]	4 (0.74)	2 (0.30)	2 (0.30)	4 (0.60)	9 (1.34)	2 (0.33)

[a] Tl^+ number is given with its occupancy in parentheses. [b] Located near the bending region. [c] Located at the same site. [d] Total number of Tl^+ ions are given with the sum of occupancies in parentheses.

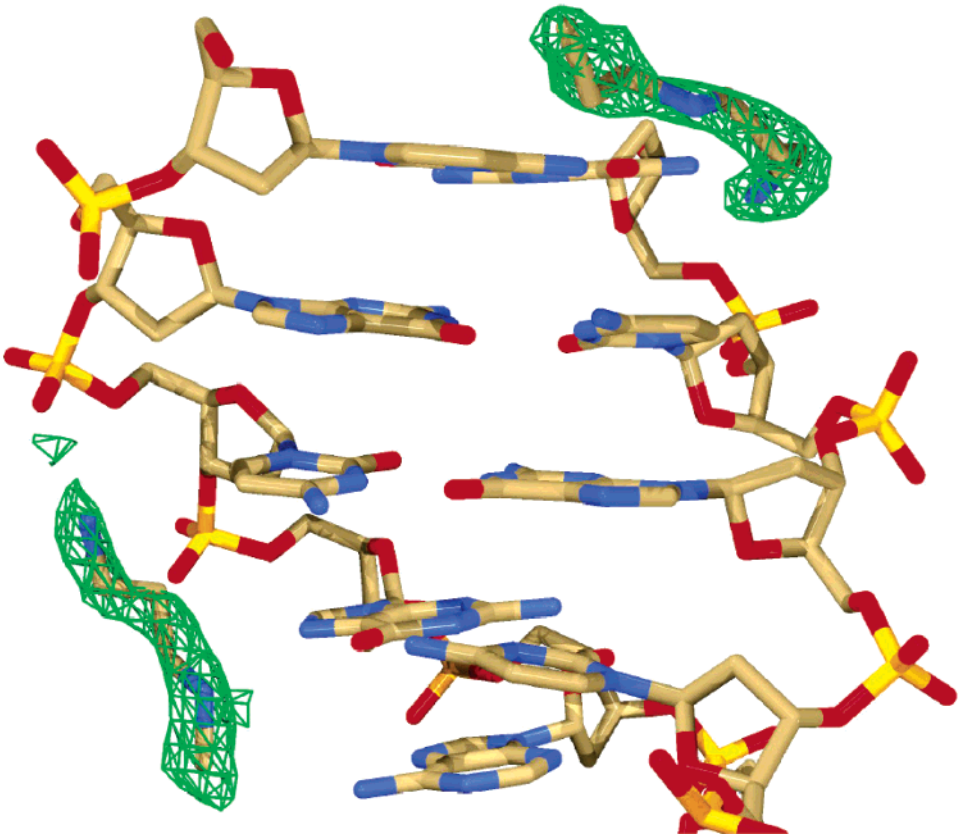

FIGURE 8: Close-up view of the sum electron density contoured at 1.0σ drawn as a cyan net around the two partial spermine molecules in the structure.

each dodecamer duplex. Three of the tethered cations are directed radially out from the DNA. This radial disposition of the tethered cations was not anticipated. Rather, we assumed, from previous behavior of polyamines (*32*, *39*, *56*, *57*), that the amino-propyl groups would lay on the floor of the major groove. The radially directed tethered cations do not appear to induce structural changes or to displace counterions. On one end of the duplex, spermine molecules and Tl^+ ions are located on the major groove floor, and in regions similar to those in DDD-Tl^+, the tethered amino groups are remote from the DNA. The DNA conformation is unperturbed.

In contrast, on the opposing end of the duplex, one of the tethered cations is directed in the 3′ direction toward a phosphate group. This tethered cation appears to interact electrostatically with the DNA. This interaction is accompanied by changes in helical parameters rise, roll, and twist and by a displacement of the backbone relative to a control oligonucleotide. In addition, these interactions appear to be associated with displacement of counterions from the major groove of the DNA.

In the NMR solution structure of the DDD^{2+}, the DNA shows 2-fold symmetry, as anticipated; the NMR structure represents a time average of the solution states of the molecule. The NMR experiment cannot distinguish between the two termini. The two amino-propyl modifications appear to behave similarly. They both appear to interact with the backbone to bend the DNA at both termini. The X-ray structure of DDD^{4+} lacks 2-fold symmetry. The end of the duplex with the greatest cation-phosphate proximity shows the greatest alteration in conformation, relative to DDD-Tl^+. Lattice forces in the crystal state create different electrostatic environments at each terminus. However, it is conceivable that the observed conformation in the crystal is a “trapped” intermediate. In solution, the distortion may be greater than in the crystal structure described here. Lattice electrostatic

forces (Figure 4) may be working in opposition to intramolecular bending forces. Further studies on how the sequence-dependent location of cations affects the DNA structure are ongoing.

It was proposed that tethered cations would form salt bridges with the O1P or O2P of the phosphates. The term "salt bridge" indicates a van der Waals contact between two atoms carrying full or partial positive and negative charges. However, the proposed conformation required for salt bridging was not confirmed by electrostatic footprinting, molecular modeling, and NMR studies. Those results support conformations where the tethered cations are oriented in the 3′ direction. The orientation of the tethered ammonium ion positions the ammonium ion near the floor of the major groove, in proximity to a G, or into the solution in a sequence-dependent manner (*30*, *58*). This orientation appears to be confirmed here. However, it should be noted that electrostatic interactions fall off gradually with distance. An absence of salt bridges does not imply an absence of strong electrostatic interaction. In summary, the structural studies are consistent with the Rouzina and Bloomfield model for the collapse of the major groove around bound cations.

ACKNOWLEDGMENT

This research was carried out in part at the APS, which is supported by the U.S. Department of Energy. The authors thank Drs. Nick Hud, Roger Wartell, Allen Orville, Angus Wilkinson, and Donald Doyle for helpful discussions.

NOTE ADDED IN PROOF

After the submission of the current manuscript, the following relevant article was published: Both, J., Brown, T., Vadhia, S. J., Lack, O., Cummins, W. J., Trent, J. O., and Lane, A. N. (2005) Determining the origin of the stabilization of DNA by 5-aminopropynylation of pyrimidine, *Biochemistry 44*, 4710−4719.

REFERENCES

1. Wing, R., Drew, H., Takano, T., Broka, C., Takana, S., Itakura, K., and Dickerson, R. E. (1980) Crystal structure analysis of a complete turn of B-DNA, *Nature 287*, 755−758.
2. Alexeev, D. G., Lipanov, A. A., and Skuratovskii, I. Y. (1987) Poly(dA)-poly(dT) is a B-type double helix with a distinctively narrow minor groove, *Nature 325*, 821−823.
3. Burkhoff, A. M., and Tullius, T. D. (1987) The unusual conformation adopted by the adenine tracts in kinetoplast DNA, *Cell 48*, 935−943.
4. Marini, J. C., Levene, S. D., Crothers, D. M., and Englund, P. T. (1982) Bent helical structure in kinetoplast DNA, *Proc. Natl. Acad. Sci. U.S.A. 79*, 7664−7668.
5. Hagerman, P. J. (1984) Evidence for the existence of stable curvature of DNA in solution, *Proc. Natl. Acad. Sci. U.S.A. 81*, 4632−4636.
6. Diekmann, S., and Wang, J. C. (1985) On the sequence determinants and flexibility of the kinetoplast DNA fragment with abnormal gel electrophoretic mobilities, *J. Mol. Biol. 186*, 1−11.
7. Drew, H. R., Wing, R. M., Takano, T., Broka, C., Itakura, K., and Dickerson, R. E. (1981) Structure of a B-DNA dodecamer. Conformation and dynamics, *Proc. Natl. Acad. Sci. U.S.A. 78*, 2179−2183.
8. Brukner, I., Susic, S., Dlakic, M., Savic, A., and Pongor, S. (1994) Physiological concentration of magnesium ions induces a strong macroscopic curvature in GGGCCC-containing DNA, *J. Mol. Biol. 236*, 26−32.
9. Dlakic, M., and Harrington, R. E. (1995) Bending and torsional flexibility of G/C-rich sequences as determined by cyclization assays, *J. Biol. Chem. 270*, 29945−29952.
10. Hud, N. V., and Plavec, J. (2003) A unified model for the origin of DNA sequence-directed curvature, *Biopolymers 69*, 144−158.
11. Wolk, S., Thurmes, W. N., Ross, W. S., Hardin, C. C., and Tinoco, I., Jr. (1989) Conformational analysis of d(C3G3), a B-family duplex in solution, *Biochemistry 28*, 2452−2459.
12. Xu, Q., Shoemaker, R. K., and Braunlin, W. H. (1993) Induction of B-A transitions of deoxyoligonucleotides by multivalent cations in dilute aqueous solution, *Biophys. J. 65*, 1039−1049.
13. Howerton, S. B., Sines, C. C., VanDerveer, D., and Williams, L. D. (2001) Locating monovalent cations in the grooves of B-DNA, *Biochemistry 40*, 10023−10031.
14. Howerton, S. B., Nagpal, A., and Williams, L. D. (2003) Surprising roles for electrostatic interactions in DNA−ligand complexes, *Biopolymers 69*, 87−99.
15. Basu, S., Rambo, R. P., Strauss-Soukup, J., Cate, J. H., Ferre-D'Amare, A. R., Strobel, S. A., and Doudna, J. A. (1998) A specific monovalent metal ion integral to the AA platform of the RNA tetraloop receptor, *Nat. Struct. Biol. 5*, 986−992.
16. Gill, H. S., and Eisenberg, D. (2001) The crystal structure of phosphinothricin in the active site of glutamine synthetase illuminates the mechanism of enzymatic inhibition, *Biochemistry 40*, 1903−1912.
17. Pedersen, P. A., Nielsen, J. M., Rasmussen, J. H., and Jorgensen, P. L. (1998) Contribution to Tl^+, K^+, and Na^+ binding of Asn776, Ser775, Thr774, Thr772, and Tyr771 in cytoplasmic part of fifth transmembrane segment in α-subunit of renal Na,K-ATPase, *Biochemistry 37*, 17818−17827.
18. Loria, J. P., and Nowak, T. (1998) Conformational changes in yeast pyruvate kinase studied by 205Tl+ NMR, *Biochemistry 37*, 6967−6974.
19. Villeret, V., Huang, S., Fromm, H. J., and Lipscomb, W. N. (1995) Crystallographic evidence for the action of potassium, thallium, and lithium ions on fructose-1,6-bisphosphatase, *Proc. Natl. Acad. Sci. U.S.A. 92*, 8916−8920.
20. Badger, J., Kapulsky, A., Gursky, O., Bhyravbhatla, B., and Caspar, D. L. (1994) Structure and selectivity of a monovalent cation binding site in cubic insulin crystals, *Biophys. J. 66*, 286−292.
21. Badger, J., Li, Y., and Caspar, D. L. (1994) Thallium counterion distribution in cubic insulin crystals determined from anomalous X-ray diffraction data, *Proc. Natl. Acad. Sci. U.S.A. 91*, 1224−1228.
22. Gursky, O., Li, Y., Badger, J., and Caspar, D. L. (1992) Monovalent cation binding to cubic insulin crystals, *Biophys. J. 61*, 604−611.
23. Gursky, O., Badger, J., Li, Y., and Caspar, D. L. (1992) Conformational changes in cubic insulin crystals in the pH range 7-11, *Biophys. J. 63*, 1210−1220.
24. Brown, I. D. (1988) What factors determine cation coordination numbers, *Acta Crystallogr., Sect. B 44*, 545−553.
25. Stroud, R. M., Kay, L. M., and Dickerson, R. E. (1974) The structure of bovine trypsin: Electron density maps of the inhibited enzyme at 5 and 2.7 Å resolution, *J. Mol. Biol. 83*, 185−208.
26. Manning, G. S., Ebralidse, K. K., Mirzabekov, A. D., and Rich, A. (1989) An estimate of the extent of folding of nucleosomal DNA by laterally asymmetric neutralization of phosphate groups, *J. Biomol. Struct. Dyn. 6*, 877−889.
27. Mirzabekov, A. D., and Rich, A. (1979) Asymmetric lateral distribution of unshielded phosphate groups in nucleosomal DNA and its role in DNA bending, *Proc. Natl. Acad. Sci. U.S.A. 76*, 1118−1121.
28. Rouzina, I., and Bloomfield, V. A. (1998) DNA bending by small, mobile multivalent cations, *Biophys. J. 74*, 3152−3164.
29. Li, Z., Huang, L., Dande, P., Gold, B., and Stone, M. P. (2002) Structure of a tethered cationic 3-aminopropyl chain incorporated into an oligodeoxynucleotide: Evidence for 3′-orientation in the major groove accompanied by DNA bending, *J. Am. Chem. Soc. 124*, 8553−8560.
30. Heystek, L. E., Zhou, H. Q., Dande, P., and Gold, B. (1998) Control over the localization of positive charge in DNA: The effect on duplex DNA and RNA stability, *J. Am. Chem. Soc. 120*, 12165−12166.
31. Otwinowski, Z. (1993) In *Data Collection and Processing*, pp 56−62, Science and Engineering Research Council, Warrington, U.K.
32. Shui, X., McFail-Isom, L., Hu, G. G., and Williams, L. D. (1998) The B-DNA dodecamer at high resolution reveals a spine of water on sodium, *Biochemistry 37*, 8341−8355.

33. Berman, H. M., Zardecki, C., and Westbrook, J. (1998) The nucleic acid database: A resource for nucleic acid science, *Acta Crystallogr., Sect. D 54*, 1095−1104.
34. Brunger, A. T., Adams, P. D., Clore, G. M., DeLano, W. L., Gros, P., Grosse-Kunstleve, R. W., Jiang, J. S., Kuszewski, J., Nilges, M., Pannu, N. S., Read, R. J., Rice, L. M., Simonson, T., and Warren, G. L. (1998) Crystallography and NMR system: A new software suite for macromolecular structure determination, *Acta Crystallogr., Sect. D 54*, 905−921.
35. Parkinson, G., Vojtechovsky, J., Clowney, L., Brunger, A. T., and Berman, H. M. (1996) New parameters for the refinement of nucleic acid-containing structures, *Acta Crystallogr., Sect. D 52*, 57−64.
36. Gelbin, A., Schneider, B., Clowney, L., Hsieh, S.-H., Olson, W. K., and Berman, H. M. (1996) Geometric parameters in nucleic acids: Sugar and phosphate constitutents, *J. Am. Chem. Soc. 118*, 519−529.
37. Clowney, L., Jain, S. C., Srinivasan, A. R., Westbrook, J., Olson, W. K., and Berman, H. M. (1996) Geometric parameters in nucleic acids: Nitrogenous bases, *J. Am. Chem. Soc. 118*, 509−518.
38. Stofer, E., and Lavery, R. (1994) Measuring the geometry of DNA grooves, *Biopolymers 34*, 337−346.
39. Shui, X., Sines, C., McFail-Isom, L., VanDerveer, D., and Williams, L. D. (1998) Structure of the potassium form of CGCGAATTCGCG: DNA deformation by electrostatic collapse around inorganic cations, *Biochemistry 37*, 16877−16887.
40. Woods, K., McFail-Isom, L., Sines, C. C., Howerton, S. B., Stephens, R. K., and Williams, L. D. (2000) Monovalent cations sequester within the A-tract minor groove of [d(CGCGAATTCGCG)]2, *J. Am. Chem. Soc. 122*, 1546−1547.
41. Sines, C. C., McFail-Isom, L., Howerton, S. B., VanDerveer, D., and Williams, L. D. (2000) Cations mediate B-DNA conformational heterogeneity, *J. Am. Chem. Soc. 122*, 11048−11056.
42. Tereshko, V., Minasov, G., and Egli, M. (1999) A "hydrat-ion" spine in a B-DNA minor groove, *J. Am. Chem. Soc. 121*, 3590−3595.
43. Hagerman, P. J. (1988) Flexibility of DNA, *Annu. Rev. Biophys. Biophys. Chem. 17*, 265−286.
44. Hagerman, K. R., and Hagerman, P. J. (1996) Helix rigidity of DNA: The meroduplex as an experimental paradigm, *J. Mol. Biol. 260*, 207−223.
45. Juo, Z. S., Chiu, T. K., Leiberman, P. M., Baikalov, I., Berk, A. J., and Dickerson, R. E. (1996) How proteins recognize the TATA box, *J. Mol. Biol. 261*, 239−254.
46. Nikolov, D. B., Chen, H., Halay, E. D., Hoffman, A., Roeder, R. G., and Burley, S. K. (1996) Crystal structure of a human TATA box-binding protein/TATA element complex, *Proc. Natl. Acad. Sci. U.S.A. 93*, 4862−4867.
47. Schultz, S. C., Shields, G. C., and Steitz, T. A. (1991) Crystal structure of a CAP−DNA complex: The DNA is bent by 90°, *Science 253*, 1001−1007.
48. van Holde, K. E., Sahasrabuddhe, C. G., and Shaw, B. R. (1974) A model for particulate structure in chromatin, *Nucleic Acids Res. 1*, 1579−1586.
49. Kornberg, R. D., and Klug, A. (1981) The nucleosome, *Sci. Am. 244*, 52−64.
50. Luger, K., Mader, A. W., Richmond, R. K., Sargent, D. F., and Richmond, T. J. (1997) Crystal structure of the nucleosome core particle at 2.8 Å resolution, *Nature 389*, 251−260.
51. Strauss, J. K., Prakash, T. P., Roberts, C., Switzer, C., and Maher, L. J. (1996) DNA bending by a phantom protein, *Chem. Biol. 3*, 671−678.
52. Strauss, J. K., and Maher, L. J. (1994) DNA bending by asymmetric phosphate neutralization, *Science 266*, 1829−1834.
53. Strauss-Soukup, J. K., and Maher, L. J. (1997) DNA bending by GCN4 mutants bearing cationic residues, *Biochemistry 36*, 10026−10032.
54. Strauss-Soukup, J. K., Rodrigues, P. D., and Maher, L. J. (1998) Effect of base composition on DNA bending by phosphate neutralization, *Biophys. Chem. 72*, 297−306.
55. Strauss-Soukup, J. K., and Maher, L. J. (1998) Electrostatic effects in DNA bending by GCN4 mutants, *Biochemistry 37*, 1060−1066.
56. Williams, L. D., Frederick, C. A., Gessner, R. V., and Rich, A. (1991) In *Molecular Conformation and Biological Interactions* (Balaram, P., and Ramaseshan, S., Eds.) pp 295−309, Indian Academy of Sciences, Bangalore, India.
57. Feuerstein, B. G., Williams, L. D., Basu, H. S., and Marton, L. J. (1991) Implications and concepts of polyamine−nucleic acid interactions, *J. Cell. Biochem. 46*, 37−47.
58. Dande, P., Liang, G. N., Chen, F. X., Roberts, C., Nelson, M. G., Hashimoto, H., Switzer, C., and Gold, B. (1997) Regioselective effect of zwitterionic DNA substitutions on DNA alkylation: Evidence for a strong side chain orientational preference, *Biochemistry 36*, 6024−6032.

BI050128Z